

Article

Probing Temperature-Dependent Recombination Kinetics in Polymer:Fullerene Solar Cells by Electric Noise Spectroscopy

Giovanni Landi ¹, Carlo Barone ^{2,*} , Costantino Mauro ², Antonietta De Sio ³,
Giovanni Carapella ², Heinz Christoph Neitzert ¹ and Sergio Pagano ²

¹ Dipartimento di Ingegneria Industriale, Università di Salerno, I-84084 Fisciano, Salerno, Italy; glandi@unisa.it (G.L.); neitzert@unisa.it (H.C.N.)

² Dipartimento di Fisica “E.R. Caianiello” and CNR-SPIN Salerno, Università di Salerno, I-84084 Fisciano, Salerno, Italy; cmauro@unisa.it (C.M.); giocar@sa.infn.it (G.C.); spagano@unisa.it (S.P.)

³ Institute of Physics, Carl von Ossietzky University of Oldenburg, 26111 Oldenburg, Germany; antonietta.de.sio@uni-oldenburg.de

* Correspondence: cbarone@unisa.it; Tel.: +39-089-968212

Received: 6 September 2017; Accepted: 21 September 2017; Published: 26 September 2017

Abstract: The influence of solvent additives on the temperature behavior of both charge carrier transport and recombination kinetics in bulk heterojunction solar cells has been investigated by electric noise spectroscopy. The observed differences in charge carrier lifetime and mobility are attributed to a different film ordering and donor-acceptor phase segregation in the blend. The measured temperature dependence indicates that bimolecular recombination is the dominant loss mechanism in the active layer, affecting the device performance. Blend devices prepared with a high-boiling-point solvent additive show a decreased recombination rate at the donor-acceptor interface as compared to the ones prepared with the reference solvent. A clear correlation between the device performance and the morphological properties is discussed in terms of the temperature dependence of the mobility-lifetime product.

Keywords: organic photovoltaics; electric noise processes; Langevin-type recombination

1. Introduction

Organic solar cells have found notable interest thanks to promising features such as low cost, flexibility, light weight, transparency, and large-area manufacturing compatibility [1]. The possibility to use a low-cost printing and roll-to-roll fabrication on flexible substrates represents, for the organic photovoltaics, a technological advancement for large scale applications. However, low power conversion efficiency and stability, when compared to inorganic technologies, still represent a limiting factor for the applicability of organic solar cells [1]. In this work, the donor-acceptor materials in bulk heterojunction-type (BHJ) devices is a blend of poly(3-hexylthiophene) (P3HT) and [6,6]-phenyl-C₆₁-butyric acid methyl ester (PCBM). For such devices, power conversion efficiencies η of about 5% have been reported [2]. The use of different combinations of donor-acceptor materials based on low band gap polymers and fullerene derivatives leads to a value of η for the organic single junction solar cell higher than 10% [1]. Recently, thanks to the addition of Fe₃O₄ nanoparticles as dopant within the P3HT:PCBM, improved efficiency of 11% has been reached [3]. It is worth noting that for organic tandem devices, η values exceeding 12% have been already observed [4].

A close intermixing between donor and acceptor materials plays a key role to ensure a high rate of charge carriers and to lower the recombination rate between electrons and holes in the blend. The loss mechanisms are mainly related to recombination of the charge-separated excitons [5].

Since recombination and transport in the active layer are influenced by the film ordering [6], in order to improve the efficiency of the BHJ solar cell it is necessary to control the nanoscale morphology of the blend by nanostructuring.

In literature, several studies report the influence of the preparation conditions, such as deposition temperature and solvent additives, on the active layer morphology [7–9]. Different experimental techniques have been applied to investigate the carrier dynamics in the BHJ solar cell (e.g., the transient absorption spectroscopy and the method of time delayed collection field) [10,11]. These techniques give a direct analysis on the charge recombination mechanisms in the polymer:fullerene solar cell. However, they do not provide information on the carrier mobility and, therefore, on the charge transport, which are usually considered inefficient in low mobility materials, such as the P3HT:PCBM blend [12]. In the BHJ solar cell, the charge carrier recombination dynamics is often found to be bimolecular and is described by Langevin's theory [13,14]. In this case, the recombination rate is proportional to the sum of the electron and hole mobilities. To date, there are only few techniques, such as the charge extraction with linearly increasing voltage measurements (CELIV) and the open circuit corrected charge carrier extraction (OTRACE), that are able to determine simultaneously the carrier mobility and lifetime in the solar cells [15]. It should be noted that the mobility-lifetime product $\mu\tau$ gives a direct measurement of the correlation between recombination and the extraction of charges.

Low-frequency noise spectroscopy is a powerful and innovative tool for the analysis of electronic transport and recombination phenomena, widely used to perform a non-destructive testing of electronic devices. In order to compare the results from the noise analysis with the data reported in literature, the most widely investigated pair of P3HT:PCBM materials in BHJ devices has been considered as a reference system. The study of charge carrier fluctuations has contributed to detect: unconventional transport processes in mixed-valence manganites [16] and in oxide heterojunctions [17], nonequilibrium and degradation effects in iron-based superconductors [18], and temperature-dependent structural modifications in polymer/carbon nanotubes composites [19–21]. Moreover, noise investigation has been used to characterize defect states and phase-transitions in crystalline silicon-based and perovskite-based solar cells [22–24]. Additionally, noise analysis has also been recently used to determine the charge carrier transport and the degradation phenomena in polymer:fullerene solar cells [25,26].

In the present study voltage-noise analysis, combined with structural and photoelectric measurements, have been performed in polymer:fullerene photovoltaic devices prepared with solvent additives. A detailed discussion of the experimental results shows that the use of solvent additives increases the mesoscopic order and crystallinity within the active layer, and induces a clear improvement of the charge carrier transport. The temperature dependence of the mobility and carrier lifetime suggests that in P3HT:PCBM blends the Langevin-type bimolecular recombination loss represents one of the major device limiting factors for the efficient extraction of the charge carriers.

2. Electric Noise: General Concepts

Noise, or fluctuations, are spontaneous random variations of physical quantities in time or, more precisely, random deviations of these quantities from some mean values that are either constant or vary nonrandomly in time. Therefore, noise is a stochastic process and is described by a random function $x(t)$. The deviation of $x(t)$ from its mean value $\langle x \rangle$ is the fluctuation $\delta x(t) = x(t) - \langle x \rangle$. The kinetics of such a fluctuation, that is how $\delta x(t)$ evolves in time on average, can be analyzed through the correlation function.

In the theory of fluctuations, an important class of random processes is composed by Gaussian processes for which the correlation function establishes the correlation between the values of the random process at two different times t_1 and t_2 . This is commonly known as the autocorrelation function $\Psi_x(t_1, t_2)$, depending only on the difference $t_1 - t_2$ in the case of stationary systems.

The autocorrelation is the main statistical function used to describe the basic properties of random data in the time domain. Similar information in the frequency domain can be obtained by the spectral

density function $S_x(f)$, which is the Fourier transform of the autocorrelation function. More in details, from the Wiener-Khintchine theorem, it follows that $S_x(f) = \Psi_x(\omega)$ and the integral of the spectral density over all positive frequencies is exactly the variance of the noise (i.e., the fluctuations amplitude).

The principal application for a power spectral density function measurement of physical data is to establish their frequency composition. This, in turn, bears important relationships to the basic characteristics of the physical system involved. The most common types of low-frequency noise in condensed matter systems are: (I) the Johnson or thermal noise, that is the electronic noise generated by the thermal agitation of the charge carriers (usually the electrons) inside an electrical conductor at equilibrium; (II) the shot noise, that is the electronic noise which can be modeled by a Poisson process and is originated from the discrete nature of electric charge; (III) the pink or $1/f$ noise, that is the electronic noise characterized by a frequency spectrum which is inversely proportional to the frequency of the signal; and (IV) the random telegraph noise, that is the electronic noise consisting of sudden step-like transitions between two or more discrete voltage or current levels. As a rule, in uniform conductors the spectral density of $1/f$ noise is proportional to the square of the mean voltage \bar{V}^2 or the mean current \bar{I}^2 . This direct proportionality has been verified many times on various conductors, and Hooge developed a qualitative rule by extrapolating a value of 2×10^{-3} as the universal proportionality noise coefficient. However, this empirical Hooge relationship has not a general physical base and, especially in complex systems such as photovoltaic devices, can not be applied (see the experimental results shown in the following section for a direct confirmation). A detailed analysis of electric noise in condensed matter can be found in [27].

3. Results

3.1. Electrical Transport and Structural Properties

The current density-voltage (J-V) characteristics under illumination of the solar cells prepared with 1,2-dichlorobenzene (oDCB) reference solvent and oDCB with 1,2,3,4-tetrahydronaphthalene (oDCB+THN) mixture solvent are shown in Figure 1a. By considering the single diode model of the solar cell, the following parameters have been extracted for oDCB based devices: short circuit current density $J_{SC} = (5.5 \pm 0.3) \text{ mA}\cdot\text{cm}^{-2}$, open circuit voltage $V_{OC} = (0.58 \pm 0.03) \text{ V}$, fill factor $FF = (69 \pm 3)\%$, and a power conversion efficiency $\eta = (2.2 \pm 0.1)\%$. The same parameters for oDCB+THN are: $J_{SC} = (7.4 \pm 0.4) \text{ mA}\cdot\text{cm}^{-2}$, $V_{OC} = (0.61 \pm 0.03) \text{ V}$, $FF = (72 \pm 3)\%$, and $\eta = (3.3 \pm 0.2)\%$. The increase of the η value for the device fabricated with the solvent mixture seems to be mainly due to the increase of the J_{SC} . Differences in the FF and V_{OC} are within the experimental errors. As can be observed, the oDCB+THN blend has a higher photocurrent, as compared to the blend prepared from pure oDCB. In Figure 1b the external quantum efficiency (EQE) spectrum for both solar cells is shown. In agreement with the J-V characteristics, the oDCB+THN blend shows a higher intensity of the EQE spectrum compared to the reference blend in the whole wavelength range. Here, the photocurrent density values evaluated from the integral of the EQE spectra are consistent with what estimated from the J-V characteristics. In particular, the resulting values of the J_{SC} are $5.5 \text{ mA}\cdot\text{cm}^{-2}$ and $7.5 \text{ mA}\cdot\text{cm}^{-2}$ for the oDCB and oDCB+THN solvent, respectively. Additionally, in the lowest EQE signal, which is related to the oDCB blend, a marked drop in the spectrum between 350 and 450 nm is observed. This behavior has been already reported in literature for the P3HT:PCBM blend when a poor ordering of the polymer is obtained during the film formation [28]. It should be noted that the use of the tetralin leads to an increase of the crystalline order in the nanoscale interpenetrating network for both the acceptor and donor components. The film ordering strongly influences the absorption spectra of the P3HT:PCBM layer. In particular, the shoulder located at 620 nm gives an indication of the P3HT crystallinity in the blend, for details see [8] and references therein. For the samples here investigated, the relative intensity of the shoulder at 620 nm appears to be more pronounced in the blend deposited from oDCB+THN [8]. This means that the use of THN additive leads to a better phase segregation of the polymer and fullerene materials in the active blend.

This finding suggests that the solar cell performance is strongly related to the morphology of the active layer due to the solvent addition.

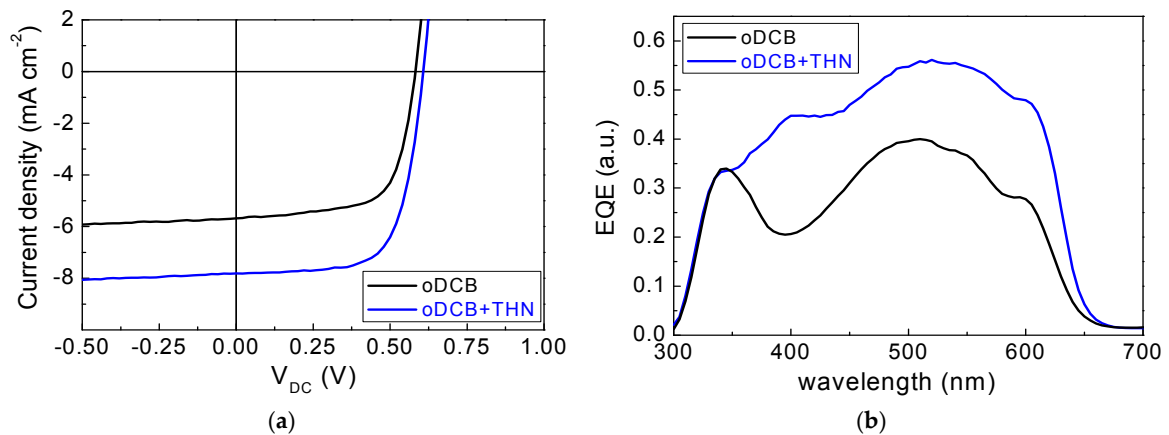


Figure 1. (a) Illuminated current density-voltage characteristics of solar cells with active layers prepared using the solvents oDCB (black line) and oDCB+THN (blue line); (b) External quantum efficiency (EQE) characteristics of solar cells with blends using the solvents oDCB (black line) and oDCB+THN (blue line).

This hypothesis is also confirmed by atomic force microscopy (AFM) analysis. In Figure 2 the AFM images for the different blends are shown. The average RMS roughness is about 1.1 nm and 4.6 nm for the blend prepared from oDCB and oDCB+THN, respectively [8]. In literature several authors report the positive correlation between increased blend surface roughness and increased solar cell efficiency in bulk heterojunction solar cells [8,29–31]. This is a further evidence of the P3HT ordering in the active layer, which leads to improvements in the photocurrent and, therefore, also in the power conversion efficiency.

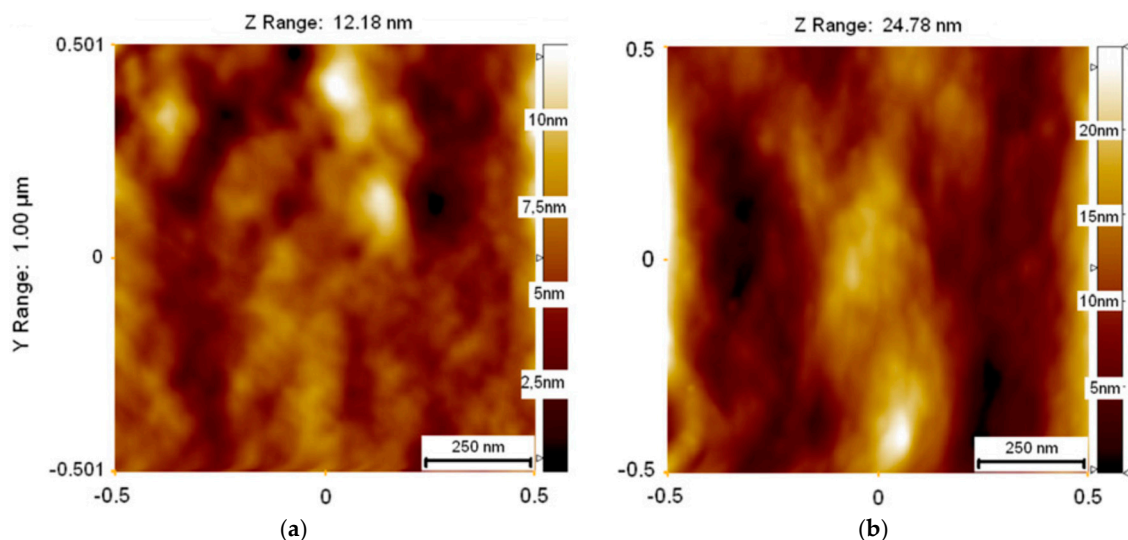


Figure 2. Atomic force microscopy images of the blends prepared using the solvents oDCB (a) and oDCB+THN (b).

3.2. Noise Properties

The study of charge carrier fluctuation mechanisms is essentially based on the measurement of the voltage-spectral density S_V generated by the device. In Figure 3 the frequency dependence of

S_V is shown for the solar cells fabricated with the reference oDCB solvent (black spectra) and with oDCB+THN (blue spectra). A similar behavior is observed at two different temperatures, as shown in Figure 3a ($T = 300$ K) and in Figure 3b ($T = 320$ K), for a fixed applied bias current $I_{DC} = 20$ μ A and measured in dark conditions.

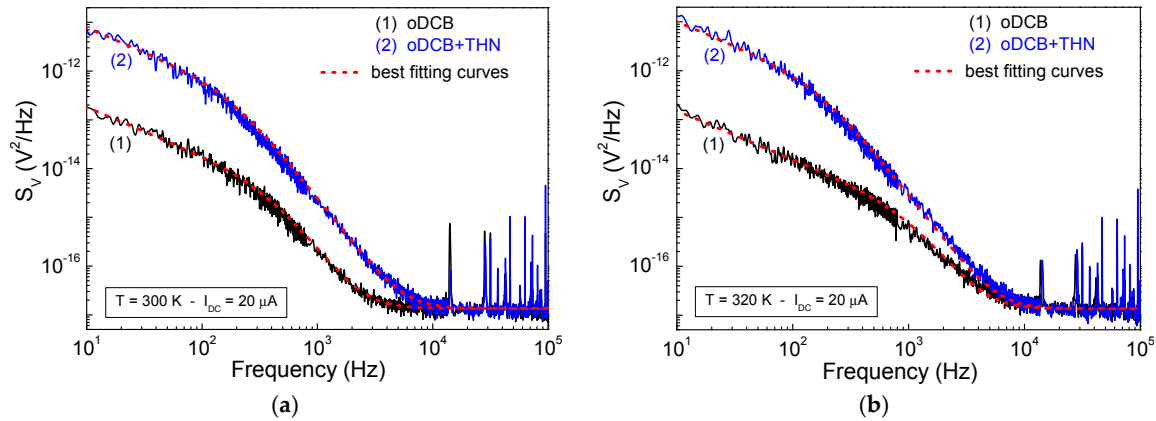


Figure 3. Low-frequency voltage-noise spectra of a device fabricated with oDCB as solvent, curves 1, and of a device fabricated with oDCB+THN as solvent, curves 2. Experimental data are measured in dark conditions at different temperatures: (a) $T = 300$ K; (b) $T = 320$ K. The dashed curves are the best fit obtained by using Equation (1).

Two distinct noise components can be identified. The first is the flicker noise $S_V^{flicker}$, which appears in the low-frequency region and is associated to electrical conductivity fluctuations [27]. The second one is the thermal noise $S_V^{thermal}$, which characterizes the high-frequency region of the spectrum and depends on temperature fluctuations of the charge carriers interacting with the polymeric chains [27]. By modeling the electronic behavior of the cells with a simple RC circuit formed by the recombination resistance R_{rec} and the chemical capacitance C_μ of the active layer [32,33], it is possible to express S_V as [25]:

$$S_V(f) = S_V^{flicker} + S_V^{thermal} = \frac{K (R_{rec} I_{DC})^2}{f^\gamma \left(1 + \left(\frac{f}{f_x}\right)^2\right)} + 4k_B T R_{rec} \quad (1)$$

In Equation (1), K is the amplitude of the flicker noise component, γ is an exponent close to unity, f_x is a cut-off frequency at which a change from a $1/f$ to a $1/f^3$ dependence of the voltage-noise spectrum is observed, and k_B is the Boltzmann constant. A good agreement between the experimental voltage-spectral density and the model of Equation (1) is shown by the red dashed curves in Figure 3. The corresponding values of the fitting parameters at $T = 300$ K are: $K = (8.5 \pm 0.6) \times 10^{-11}$, $f_x = (199 \pm 6)$ Hz, and $\gamma = (1.00 \pm 0.02)$ for the trace 1; while: $K = (1.4 \pm 0.1) \times 10^{-9}$, $f_x = (133 \pm 4)$ Hz, and $\gamma = (1.00 \pm 0.02)$ for the trace 2. The cut-off frequency shifts to lower frequencies and the value of K increases when the THN solvent is added to the solution. It is worth noting that when increasing the temperature, the noise amplitude remains almost constant whereas the cut-off frequency shifts to higher frequencies.

The best fitting values of the parameter f_x can be used to estimate the effective carrier lifetime as:

$$\tau = (2\pi f_x)^{-1} = (2\pi R_{rec} C_\mu)^{-1} \quad (2)$$

By defining the recombination resistance of electrons and holes as $R_{rec} = (dV_F/dI_{DC})$ [34], from Equation (2) it is straightforward to compute the lifetime dependence on the forward bias voltage V_F , that is the dc voltage without the contribution of the device series resistance [35]. The experimental values for τ are shown in Figure 4 at different temperatures between 300 and 330 K and for the two types of solar cells investigated (oDCB solvent in pink region and oDCB+THN solvent in blue region).

As clearly evident in Figure 4, the use of the THN as solvent leads to an increase of τ . Indeed, at 300 K the observed effective lifetime ranges between 1.2 and 0.6 ms for the blend fabricated with the solvent mixture oDCB+THN. On the other hand, the devices prepared by using the reference solvent show lower values of τ , ranging between 0.8 and 0.2 ms. In literature are reported similar values of the charge carrier lifetimes, measured with alternative experimental techniques such as impedance spectroscopy and photo-induced absorption [36,37]. Additionally, a decrease of τ with an increase of the bias voltage, corresponding to an increase of the charge carriers stored within the organic device, has been observed at all the investigated temperatures and for both types of used solvents. This suggests that the recombination dynamics of the blend seems to be bimolecular, as the effective lifetime τ depends on the charge carrier concentration n [15]. The lower values obtained for the device fabricated with the reference solvent (full symbols in Figure 4) indicate a strong recombination in the blend. Conversely, higher values of τ , as observed for the device prepared with the addition of THN (open symbols in Figure 4), are indicative for a more efficient charge carrier transport in the active layer. It seems that the solvent mixture leads to a reduced charge carrier recombination rate, thus leading to an increase of the carrier lifetime. This is in good agreement with the measurements on the electrical transport and the structural properties shown in Figures 1 and 2. It is worth noting that for both the investigated devices, the carrier lifetime decreases with increasing temperature. This is a further evidence that the dominant recombination losses within the device could be Langevin-type bimolecular recombination [13].

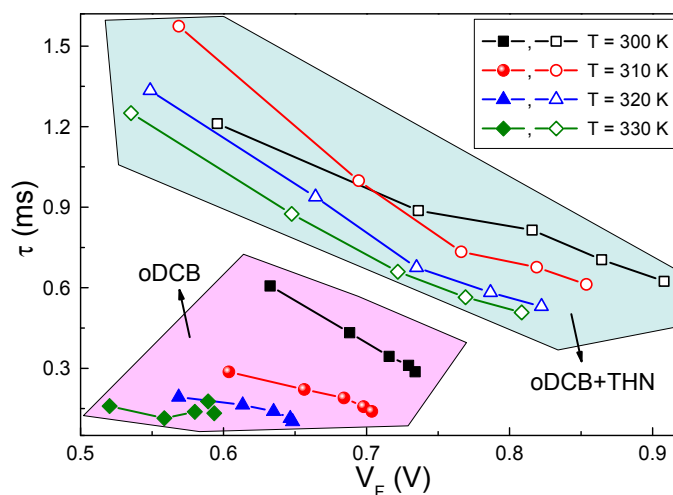


Figure 4. Effective carrier lifetime dependence on the forward voltage, at temperatures between 300 and 330 K. The experimental data are directly extracted by noise measurements. Full symbols refer to the oDCB solvent (pink region), while open symbols refer to the oDCB+THN solvent (blue region).

4. Discussion

In order to investigate the influence of the solvent on the film ordering in the blend and hence on the charge carrier transport, an evaluation of the carrier mobility from voltage-noise measurements has been made. As reported in literature, the mobility can be computed from the amplitude of flicker and thermal noise components as [38]:

$$\mu = \frac{k_B T}{e \tau E^2} \int_{f_{min}}^{f_{max}} \frac{S_V^{flicker}(f)}{S_V^{thermal}} df \tag{3}$$

where e is the elementary charge, τ is the carrier lifetime as defined in Equation (2), $E = V_F/t$ is the applied electric field (being t the active layer thickness), and $[f_{min}, f_{max}]$ is the experimental frequency bandwidth. The values obtained from Equation (3) are shown in Figure 5. At all temperatures, a clear

reduction of μ is evident for the cells with the oDCB+THN solvent (open symbols in blue region) upon respect to the reference solvent oDCB (full symbols in pink region). From this analysis, it is not possible to distinguish between electron and hole transport. However, it is well-known that in P3HT:PCBM blends the electron mobility is usually higher than the hole mobility [39,40]. Therefore, the experimental data of Figure 5 can be attributed to the electrons in the blends. The observed increase of μ with temperature and its bias dependence suggest that the dominant carrier transport mechanism is a thermally assisted hopping process between localized charge transport sites [13]. This conduction mechanism has been already found in diodes, field effect transistors, and in solar cells based on organic and inorganic disordered materials such as perovskites, small molecules and conjugated polymers [41–45].

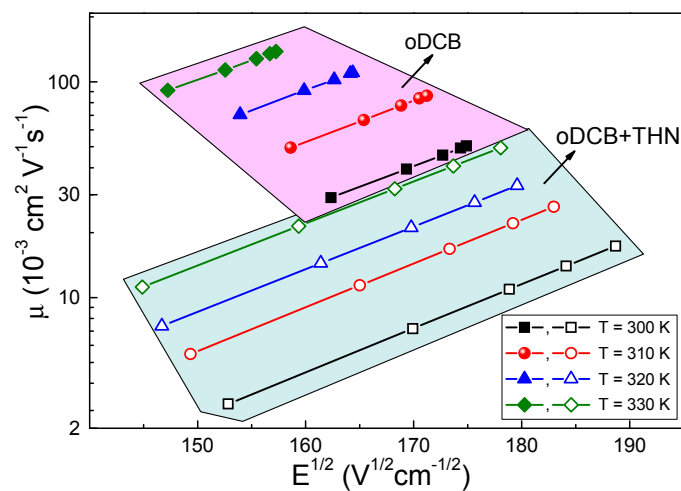


Figure 5. Electron mobility dependence, obtained by noise analysis, on the square root of the applied electric field. The best fitting curves (solid lines) are derived from the Poole-Frenkel model of Equation (4), both for the oDCB solvent (full symbols) and the oDCB+THN solvent (open symbols).

Figure 5 also shows an exponential dependence of μ on $E^{1/2}$, that can be interpreted in terms of the Poole-Frenkel model as [46]:

$$\mu = \mu_0 \exp \left[\frac{e^{3/2}}{2k_B} \left(\frac{E}{\pi \epsilon_0 \epsilon_r} \right)^{1/2} \frac{1}{T_{eff}} \right] \quad (4)$$

In Equation (4), ϵ_0 is the vacuum permittivity, $\epsilon_r \approx 3$ is the relative dielectric constant for P3HT:PCBM [36], μ_0 is the zero-field mobility, and $T_{eff}^{-1} = T^{-1} - T_{Gill}^{-1}$ is related to the Gill temperature at which the mobility is independent of the electric field. The best fitting curves, obtained from Equation (4) with μ_0 and T_{eff} as free fitting parameters, are shown in Figure 5 as solid lines. A good agreement between the model and the experimental data is clearly evident, thus confirming the validity of the theoretical framework of Equation (4) in describing the electric transport of organic devices [45,47]. In particular, the carrier transport within the blend occurs by pathways along nearest sites, located on the polymer and fullerene phases for the holes and electrons, respectively, by overcoming an energetic barrier. An accurate estimation of the average value of the hopping barrier for the electrons can be performed by taking into account the Gill energy defined as $E_{Gill} = k_B T_{Gill}$ [26]. The temperature dependencies of μ_0 and of E_{Gill} are reported in Figure 6 and are related to thermal activated processes within the active layer [26]. As visible in Figure 6, the use of the solvent mixture during the deposition phase produces a negligible change of E_{Gill} , of less than 3%. More in details, the estimated room temperature value of E_{Gill} is (54 ± 1) meV and (56 ± 1) meV for the reference and for the oDCB+THN solvent, respectively. These values are consistent with those reported in literature for BHJ solar cells,

characterized by the formation of a neat P3HT layer under the cathode during thermally induced aging [26].

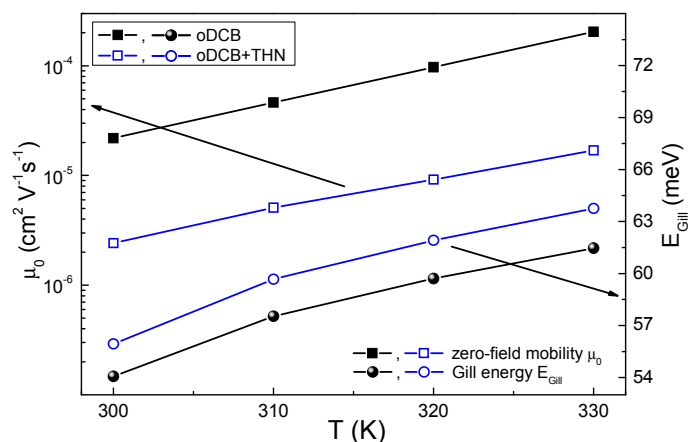


Figure 6. Temperature dependence of the zero-field mobility (left y -axis) and of the Gill energy (right y -axis). Full and open symbols correspond to oDCB and oDCB+THN solvent, respectively.

The zero-field mobility (left y -axis in Figure 6), obtained by noise measurements at 300 K of oDCB based devices, is $\mu_0 = (22 \pm 1) \times 10^{-6} \text{ cm}^2 \cdot \text{V}^{-1} \cdot \text{s}^{-1}$ and is in good agreement with the value measured by using charge extraction with linearly increasing voltage measurements in similar samples [8]. On the other hand, the zero-field mobility for the device prepared by using oDCB+THN solvent is $\mu_0 = (2.4 \pm 0.1) \times 10^{-6} \text{ cm}^2 \cdot \text{V}^{-1} \cdot \text{s}^{-1}$, lower than what found by using oDCB as solvent. This is consistent with the observed increased mesoscopic ordering in the blend. As already reported in literature, the blend casted from a high-boiling-point solvent, as the oDCB+THN, has a higher polymer crystallinity in the active layer as compared to the blend prepared with a low-boiling-point solvent, as the oDCB [8,48]. Indeed, the increase of the film ordering induces a vertical phase separation between polymer and fullerene materials which causes a diffusion out of the PCBM material within the blend [49]. The formation of a polymer rich phase reduces the charge carrier transfer and, therefore, also the zero-field electron mobility decreases for the blend prepared with the mixture solvent. However, it is worth noting that the device prepared by using the oDCB+THN solvent shows a higher photocurrent value and, as a consequence, a higher conversion efficiency as compared to the solar cell fabricated with the reference solvent only. In polymer:fullerene solar cells, the photocurrent is due to the light absorption in the active layer with the subsequent generation of excitons. The use of THN influences the phase segregation within the blend with a negligible effect on the optical properties. It has already been verified that for the thicknesses of the blends investigated in this study (115 nm for oDCB and 130 nm for oDCB+THN) only a minimal difference in the short circuit current density is obtained [8]. Therefore, the difference in the J_{SC} values can be fundamentally related to the recombination and transport mechanisms in the solar cell.

4.1. Solvent Influence on the Charge Carrier Recombination Process

In semiconductor materials the charge carrier recombination process in the bulk is well described by the Langevin theory [14]. The associated recombination rate can be expressed by $R_L = \beta(np - n_i^2)$, where n and p are electron and hole concentrations, respectively, and n_i is the intrinsic carrier concentration. The Langevin recombination factor is defined as:

$$\beta = \frac{e}{\epsilon_r \epsilon_0} (\mu_n + \mu_h) \quad (5)$$

where e is the elementary charge, $\epsilon_r \epsilon_0$ the effective dielectric constant of the ambipolar semiconductor, and μ_n and μ_h are the electron and hole mobilities. By assuming that the recombination processes at the metal electrodes are negligible and by considering that the holes are solely transported in the donor polymer phase and electrons through the fullerene acceptor, a bimolecular recombination can only take place at the heterojunction. Since $\mu_n \gg \mu_h$, Equation (5) can be written as $\beta \approx \frac{e}{\epsilon_r \epsilon_0} \mu$, where $\mu \approx \mu_n$ is the higher carrier mobility value (the electron one, shown in Figure 5). At room temperature, $\beta = (17.6 \pm 0.4) \times 10^{-9} \text{ cm}^3 \cdot \text{s}^{-1}$ and $\beta = (4.3 \pm 0.1) \times 10^{-9} \text{ cm}^3 \cdot \text{s}^{-1}$ can be computed for the oDCB and oDCB+THN solvent, respectively. These values are in good agreement with typical recombination factors reported in literature for various organic solar cells [12,50]. As already evidenced, the use of THN reduces the recombination rate at the hetero-interface between the donor and the acceptor phases, leading to an increase of the carrier lifetime. Conversely, for the reference solvent a higher mobility increases the probability of finding the opposite charge carrier, thus enhancing the charge recombination. This finding is fully consistent with the assumption that the bimolecular recombination loss is one of the major device efficiency limiting factors in the P3HT:PCBM blend prepared with different solvents. The decrease of τ values as a function of the temperature is expected by the Langevin theory, because lower temperatures reduce the carrier mobility and, consequently, the recombination rate R_L of the carriers is lowered [13].

4.2. Solvent Influence on the Charge Carrier Extraction

In order to evaluate the charge carrier extraction from the investigated devices, the mobility-lifetime product $\mu\tau$ has been calculated and analyzed as a function of the bias current injection level. This figure of merit gives a direct information about the competition between the charge carrier transport and the recombination mechanisms in the active layer. Both processes have a large impact on the voltage bias dependence of the photocurrent and hence on the efficiency of the solar cell [15]. As evident in Figure 5, the charge mobility is directly proportional to the temperature for both the used solvents. On the contrary, Figure 4 shows that the charge carrier lifetime is inversely proportional to the temperature. According to the Langevin-type bimolecular recombination theory, $\mu\tau$ should be independent of the temperature [13].

In Figure 7, the values of $\mu\tau$, measured between 300 and 330 K, for different bias currents, and in dark condition, are reported as Arrhenius plots for the reference and the mixture solvents. As can be observed in Figure 7a for the reference solvent, the $\mu\tau$ product (at low current injection levels, that is 20 μA and 30 μA) shows a temperature-independent value of about $15 \times 10^{-6} \text{ cm}^2 \cdot \text{V}^{-1}$, consistent with that reported in literature [15]. By increasing the current, the charge amount n , accumulated in the device, increases and the mobility-lifetime product becomes temperature dependent. In particular, with a bias current of 50 μA , corresponding to a charge density of 10^{16} cm^{-3} within the active layer, the $\mu\tau$ parameter decreases of one order of magnitude reaching a value of about $10^{-6} \text{ cm}^2 \cdot \text{V}^{-1}$. This suggests that the charge extraction process is less efficient for the device prepared with the reference solvent. This is also supported by the lower value of J_{SC} observed for this device (Figure 1a). The existence of additional recombination pathways at the heterojunction between the donor and the acceptor materials leads to an increase of the carrier recombination dynamics. In literature several studies report that the recombination dynamics at the hetero-interface can be influenced by the presence of the charge accumulation and energetic disorder [14,51].

On the other hand, the active layer prepared by using THN as additive shows an approximately temperature-independent behavior of the $\mu\tau$ product with an average value of about $20 \times 10^{-6} \text{ cm}^2 \cdot \text{V}^{-1}$ (similar to that observed for the oDCB) in the whole investigated current range. The reduction in carrier mobility results in a longer carrier lifetime, as expected in Langevin-type bimolecular recombination, where the recombination rate R_L is determined by the charge velocity (i.e., the mobility). This result is consistent with the assumption that the use of the high-boiling-point additive affects positively the morphology thereby increasing the mesoscopic ordering in the donor

and acceptor phases. This leads to a reduction of the recombination, as evidenced by enhanced phase segregation in the blends prepared with mixed solvents.

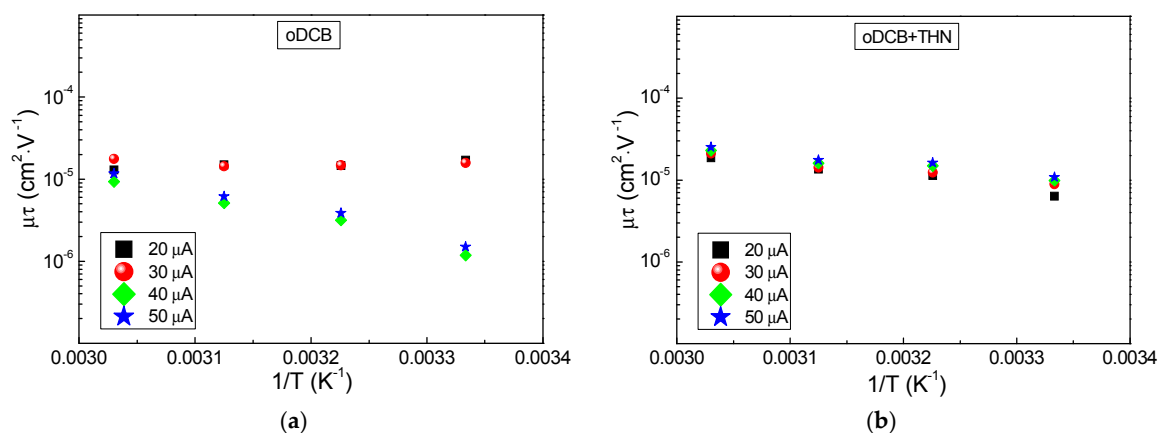


Figure 7. Temperature dependence of the mobility-lifetime products for the blend prepared by using: (a) oDCB reference solvent; (b) oDCB+THN solvent.

5. Materials and Methods

To prepare the active layers, 1,2-dichlorobenzene (oDCB, boiling-point 180 °C) was used as the host solvent, whereas 1,2,3,4-tetrahydronaphthalene (THN, boiling-point 207 °C) was the additive (10% of the entire volume). Solutions containing only the host solvent oDCB were used to prepare the reference samples. Since the solubility of P3HT and PCBM in the two solvents is slightly different [52], one expects an effect on the ordering of the blend films. P3HT (supplied from Merck Chemicals Ltd) and PCBM (purchased from Solenne BV) were dissolved in oDCB or in oDCB+THN in a 1:1 ratio in weight and stirred at 70 °C overnight before use [8]. The whole sample preparation took place in a nitrogen filled glovebox. Indium tin oxide (ITO) coated glass substrates (from PGO) were used as the anode. The substrates were patterned, cleaned in isopropyl alcohol, and exposed to an oxygen plasma. A layer of poly(3,4-ethylenedioxythiophene) (PEDOT):poly(styrenesulfonate) (PSS) (Clevios P VP Al 4083 from H.C. Starck) was then spun on top of the ITO and dried for 10 min at 180 °C. The active layer was spun on top of the PEDOT:PSS layer and annealed for 10 min at 150 °C. The film thicknesses were determined using a Veeco Dektak 6M Profilometer, resulting in values of 115 nm for oDCB and 130 nm for oDCB+THN. The thickness of the PEDOT:PSS layer was about 60 nm. The cathode was deposited by thermal evaporation of Ca and Al. The active area of the devices was 0.5 cm^2 . The investigated device structure with the following layer sequence glass/ITO/PEDOT:PSS/P3HT:PCBM/Ca/Al is shown in Figure 8.

Atomic force microscopy (AFM) analyses were performed in a UHV-STM/AFM from Omicron with a pressure below 5×10^{-10} mbar to avoid the effects of oxygen and humidity on the surface of the sample. Measurements were realized using a controller from Nanonis. Pt/Ir cantilevers from the company Nanosensors were calibrated before each measurement using a gold single crystal with 111-orientation as a reference [8].

To record the J-V characteristics, the devices were illuminated with a KH Steuernagel solar simulator providing the standard reference spectrum AM1.5 G. A reference silicon solar cell provided by Fraunhofer ISE (Freiburg, Germany) was used for the calibration. EQE was measured with a Xe-Hg tandem lamp using a 2 grating monochromator. A calibrated silicon photodetector was used to monitor the incident photon flux. The photocurrent of the device was recorded by means of a lock-in amplifier.

The temperature-dependent noise investigations were carried out by using a thermoelectric cooler Peltier-type device, with an operating range from 280 to 340 K. A LM35 sensor in contact with the sample holder was used to measure the temperature, whose stabilization, better than 1 K, was realized

through a computer-controlled feedback loop. The solar cells were biased with a low-noise Keithley dc current source. The output ac voltage signal was amplified with a low-noise Signal Recovery 5113 preamplifier and, subsequently, was analyzed with a dynamic signal analyzer HP35670A. Unwanted contact noise contributions were removed by resorting to a specific procedure, based on a sequence of two- and four-probe measurements. This technique systematically minimizes the electrical noise due to external spurious sources, while leaving unaltered the instrumental background noise level of $1.4 \times 10^{-17} \text{ V}^2/\text{Hz}$ [53].



Figure 8. Sketch of the investigated polymer:fullerene solar cells. Sixteen devices have been fabricated and analyzed for each solvent-type.

6. Conclusions

The influence of the solvent additives on the performance of polymer:fullerene solar cells has been investigated by using temperature-dependent fluctuation spectroscopy under dark conditions. The increase of the measured external quantum efficiency signal for the device prepared with the solvent additive is due to an increase of the polymer ordering within the blend. This leads to an increase of the short circuit current and, as a consequence, of the power conversion efficiency. Such a result is also confirmed by the surface analysis performed by using atomic force microscopy measurements, that indicate a connection between an increase of the device performance and the increase of the surface roughness. The observed temperature dependencies of the charge carrier lifetime and mobility suggest that the recombination kinetics, occurring within the blend, is bimolecular and follows the Langevin theory. In particular, the carrier lifetime shows a temperature-induced reduction, while the carrier mobility increases with increasing temperature, generating an evident enhancement of the carrier recombination rate. In this respect, the use of a high-boiling-point solvent (such as THN) reduces the recombination rate at the donor-acceptor interface and this leads to an increase of the carrier lifetime in the films. On the other hand, samples prepared with the reference solvent (oDCB) present higher mobility, which seems to affect the charge recombination process.

According to the Langevin theory, devices characterized with a well-ordered blend structure show temperature-independent mobility-lifetime products and, consequently, a more efficient carrier extraction process. Conversely, blends prepared with a less-ordered active layer are characterized by an increased recombination rate at the donor-acceptor interface (essentially due to the charge accumulation and energetic disorder), which leads to a decrease of the mobility-lifetime products.

Acknowledgments: This work is partially supported by University of Salerno through grants FARB14CAVAL, FARB15PAGAN, and FARB16CAVAL. Technical support of Salvatore Abate (CNR-SPIN Salerno, Italy) is gratefully acknowledged. Thomas Madena and Jürgen Parisi are also kindly acknowledged for their valuable contributions.

Author Contributions: All the authors conceived and designed the experiments; G.L., C.B., C.M. and S.P. performed the experiments; G.L., H.C.N. and G.C. analyzed the data; A.D.S. prepared photovoltaic devices; G.L. and C.B. wrote the paper with input from all co-authors.

Conflicts of Interest: The authors declare no conflict of interest.

References

1. Zhao, J.; Li, Y.; Yang, G.; Jiang, K.; Lin, H.; Ade, H.; Ma, W.; Yan, H. Efficient organic solar cells processed from hydrocarbon solvents. *Nat. Energy* **2016**, *1*, 15027. [[CrossRef](#)]
2. Zhao, G.; He, Y.; Li, Y. 6.5% Efficiency of polymer solar cells based on poly(3-hexylthiophene) and indene-C₆₀ bisadduct by device optimization. *Adv. Mater.* **2010**, *22*, 4355–4358. [[CrossRef](#)] [[PubMed](#)]
3. González, D.M.; Körstgens, V.; Yao, Y.; Song, L.; Santoro, G.; Roth, S.V.; Müller-Buschbaum, P. Improved power conversion efficiency of P3HT:PCBM organic solar cells by strong spin-orbit coupling-induced delayed fluorescence. *Adv. Energy Mater.* **2015**, *5*, 1401770. [[CrossRef](#)]
4. Li, M.; Gao, K.; Wan, X.; Zhang, Q.; Kan, B.; Xia, R.; Liu, F.; Yang, X.; Feng, H.; Ni, W.; et al. Solution-processed organic tandem solar cells with power conversion efficiencies > 12%. *Nat. Photonics* **2016**, *11*, 85–90. [[CrossRef](#)]
5. Cowan, S.R.; Roy, A.; Heeger, A.J. Recombination in polymer-fullerene bulk heterojunction solar cells. *Phys. Rev. B* **2010**, *82*, 245207. [[CrossRef](#)]
6. Hallermann, M.; Kriegel, I.; Da Como, E.; Berger, J.M.; von Hauff, E.; Feldmann, J. Charge transfer excitons in polymer/fullerene blends: The role of morphology and polymer chain conformation. *Adv. Funct. Mater.* **2009**, *19*, 3662–3668. [[CrossRef](#)]
7. Collins, B.A.; Gann, E.; Guignard, L.; He, X.; McNeill, C.R.; Ade, H. Molecular miscibility of polymer–fullerene blends. *J. Phys. Chem. Lett.* **2010**, *1*, 3160–3166. [[CrossRef](#)]
8. De Sio, A.; Madena, T.; Huber, R.; Parisi, J.; Neyshtadt, S.; Deschler, F.; Da Como, E.; Esposito, S.; von Hauff, E. Solvent additives for tuning the photovoltaic properties of polymer–fullerene solar cells. *Sol. Energy Mater. Sol. Cells* **2011**, *95*, 3536–3542. [[CrossRef](#)]
9. Jeon, N.J.; Noh, J.H.; Kim, Y.C.; Yang, W.S.; Ryu, S.; Seok, S.I. Solvent engineering for high-performance inorganic–organic hybrid perovskite solar cells. *Nat. Mater.* **2014**, *13*, 897–903. [[CrossRef](#)] [[PubMed](#)]
10. Clarke, T.M.; Jamieson, F.C.; Durrant, J.R. Transient absorption studies of bimolecular recombination dynamics in polythiophene/fullerene blend films. *J. Phys. Chem. C* **2009**, *113*, 20934–20941. [[CrossRef](#)]
11. Offermans, T.; Meskers, S.C.J.; Janssen, R.A.J. Time delayed collection field experiments on polymer:Fullerene bulk-heterojunction solar cells. *J. Appl. Phys.* **2006**, *100*, 074509. [[CrossRef](#)]
12. Fallahpour, A.H.; Di Carlo, A.; Lugli, P. Sensitivity of the drift-diffusion approach in estimating the power conversion efficiency of bulk heterojunction polymer solar cells. *Energies* **2017**, *10*, 285. [[CrossRef](#)]
13. Vijila, C.; Singh, S.P.; Williams, E.; Sonar, P.; Pivrikas, A.; Philippa, B.; White, R.; Naveen Kumar, E.; Gomathy Sandhya, S.; Gorelik, S.; et al. Relation between charge carrier mobility and lifetime in organic photovoltaics. *J. Appl. Phys.* **2013**, *114*, 184503. [[CrossRef](#)]
14. Liu, Y.; Zojer, K.; Lassen, B.; Kjelstrup-Hansen, J.; Rubahn, H.-G.; Madsen, M. Role of the charge-transfer state in reduced Langevin recombination in organic solar cells: A theoretical study. *J. Phys. Chem. C* **2015**, *119*, 26588–26597. [[CrossRef](#)] [[PubMed](#)]
15. Baumann, A.; Lormann, J.; Rauh, D.; Deibel, C.; Dyakonov, V. A new approach for probing the mobility and lifetime of photogenerated charge carriers in organic solar cells under real operating conditions. *Adv. Mater.* **2012**, *24*, 4381–4386. [[CrossRef](#)] [[PubMed](#)]
16. Savo, B.; Barone, C.; Galdi, A.; Di Trollo, A. DC transport properties and resistance fluctuation processes in Sr₂FeMoO₆ polycrystalline thin films. *Phys. Rev. B* **2006**, *73*, 094447. [[CrossRef](#)]
17. Barone, C.; Romeo, F.; Galdi, A.; Orgiani, P.; Maritato, L.; Guarino, A.; Nigro, A.; Pagano, S. Universal origin of unconventional 1/f noise in the weak-localization regime. *Phys. Rev. B* **2013**, *87*, 245113. [[CrossRef](#)]
18. Barone, C.; Pagano, S.; Pallecchi, I.; Bellingeri, E.; Putti, M.; Ferdeghini, C. Thermal and voltage activated excess 1/f noise in FeTe_{0.5}Se_{0.5} epitaxial thin films. *Phys. Rev. B* **2011**, *83*, 134523. [[CrossRef](#)]
19. Barone, C.; Pagano, S.; Neitzert, H.C. Effect of concentration on low-frequency noise of multiwall carbon nanotubes in high-density polyethylene matrix. *Appl. Phys. Lett.* **2010**, *97*, 152107. [[CrossRef](#)]

20. Barone, C.; Pagano, S.; Neitzert, H.C. Transport and noise spectroscopy of MWCNT/HDPE composites with different nanotube concentrations. *J. Appl. Phys.* **2011**, *110*, 113716. [[CrossRef](#)]
21. Barone, C.; Landi, G.; Mauro, C.; Neitzert, H.C.; Pagano, S. Universal crossover of the charge carrier fluctuation mechanism in different polymer/carbon nanotubes composites. *Appl. Phys. Lett.* **2015**, *107*, 143106. [[CrossRef](#)]
22. Landi, G.; Barone, C.; Mauro, C.; Neitzert, H.C.; Pagano, S. A noise model for the evaluation of defect states in solar cells. *Sci. Rep.* **2016**, *6*, 29685. [[CrossRef](#)] [[PubMed](#)]
23. Barone, C.; Lang, F.; Mauro, C.; Landi, G.; Rappich, J.; Nickel, N.H.; Rech, B.; Pagano, S.; Neitzert, H.C. Unravelling the low-temperature metastable state in perovskite solar cells by noise spectroscopy. *Sci. Rep.* **2016**, *6*, 34675. [[CrossRef](#)] [[PubMed](#)]
24. Landi, G.; Neitzert, H.C.; Barone, C.; Mauro, C.; Lang, F.; Albrecht, S.; Rech, B.; Pagano, S. Correlation between electronic defect states distribution and device performance of perovskite solar cells. *Adv. Sci.* **2017**, in press. [[CrossRef](#)]
25. Landi, G.; Barone, C.; De Sio, A.; Pagano, S.; Neitzert, H.C. Characterization of polymer:Fullerene solar cells by low-frequency noise spectroscopy. *Appl. Phys. Lett.* **2013**, *102*, 223902. [[CrossRef](#)]
26. Barone, C.; Landi, G.; De Sio, A.; Neitzert, H.C.; Pagano, S. Thermal ageing of bulk heterojunction polymer solar cells investigated by electric noise analysis. *Sol. Energy Mater. Sol. Cells* **2014**, *122*, 40–45. [[CrossRef](#)]
27. Kogan, S. *Electronic Noise and Fluctuations in Solids*, 1st ed.; Cambridge University Press: Cambridge, UK, 1996; ISBN 978-0521460347.
28. Yang, X.; Loos, J.; Veenstra, S.C.; Verhees, W.J.H.; Wienk, M.M.; Kroon, J.M.; Michels, M.A.J.; Janssen, R.A.J. Nanoscale morphology of high-performance polymer solar cells. *Nano Lett.* **2005**, *5*, 579–583. [[CrossRef](#)] [[PubMed](#)]
29. Chen, F.-C.; Tseng, H.-C.; Ko, C.-J. Solvent mixtures for improving device efficiency of polymer photovoltaic devices. *Appl. Phys. Lett.* **2008**, *92*, 103316. [[CrossRef](#)]
30. Li, G.; Shrotriya, V.; Huang, J.; Yao, Y.; Moriarty, T.; Emery, K.; Yang, Y. High-efficiency solution processable polymer photovoltaic cells by self-organization of polymer blends. *Nat. Mater.* **2005**, *4*, 864–868. [[CrossRef](#)]
31. Yao, Y.; Hou, J.; Xu, Z.; Li, G.; Yang, Y. Effects of solvent mixtures on the nanoscale phase separation in polymer solar cells. *Adv. Funct. Mater.* **2008**, *18*, 1783–1789. [[CrossRef](#)]
32. Ripolles-Sanchis, T.; Guerrero, A.; Bisquert, J.; Garcia-Belmonte, G. Diffusion-recombination determines collected current and voltage in polymer:Fullerene solar cells. *J. Phys. Chem. C* **2012**, *116*, 16925–16933. [[CrossRef](#)]
33. Perrier, G.; de Bettignies, R.; Berson, S.; Lemaître, N.; Guillerez, S. Impedance spectrometry of optimized standard and inverted P3HT-PCBM organic solar cells. *Sol. Energy Mater. Sol. Cells* **2012**, *101*, 210–216. [[CrossRef](#)]
34. Boix, P.P.; Guerrero, A.; Marchesi, L.F.; Garcia-Belmonte, G.; Bisquert, J. Current-voltage characteristics of bulk heterojunction organic solar cells: Connection between light and dark curves. *Adv. Energy Mater.* **2011**, *1*, 1073–1078. [[CrossRef](#)]
35. Guerrero, A.; Ripolles-Sanchis, T.; Boix, P.P.; Garcia-Belmonte, G. Series resistance in organic bulk-heterojunction solar devices: Modulating carrier transport with fullerene electron traps. *Org. Electron.* **2012**, *13*, 2326–2332. [[CrossRef](#)]
36. Garcia-Belmonte, G.; Munar, A.; Barea, E.M.; Bisquert, J.; Ugarte, I.; Pacios, R. Charge carrier mobility and lifetime of organic bulk heterojunctions analyzed by impedance spectroscopy. *Org. Electron.* **2008**, *9*, 847–851. [[CrossRef](#)]
37. Dennler, G.; Mozer, A.J.; Juška, G.; Pivrikas, A.; Österbacka, R.; Fuchsbaauer, A.; Sariciftci, N.S. Charge carrier mobility and lifetime versus composition of conjugated polymer/fullerene bulk-heterojunction solar cells. *Org. Electron.* **2006**, *7*, 229–234. [[CrossRef](#)]
38. Bonavolontà, C.; Albonetti, C.; Barra, M.; Valentino, M. Electrical mobility in organic thin-film transistors determined by noise spectroscopy. *J. Appl. Phys.* **2011**, *110*, 093716. [[CrossRef](#)]
39. Pivrikas, A.; Sariciftci, N.S.; Juška, G.; Österbacka, R. A review of charge transport and recombination in polymer/fullerene organic solar cells. *Prog. Photovolt. Res. Appl.* **2007**, *15*, 677–696. [[CrossRef](#)]
40. Lorrmann, J.; Badada, B.H.; Inganäs, O.; Dyakonov, V.; Deibel, C. Charge carrier extraction by linearly increasing voltage: Analytic framework and ambipolar transients. *J. Appl. Phys.* **2010**, *108*, 113705. [[CrossRef](#)]

41. Brus, V.V.; Lang, F.; Bundesmann, J.; Seidel, S.; Denker, A.; Rech, B.; Landi, G.; Neitzert, H.C.; Rappich, J.; Nickel, N.H. Defect dynamics in proton irradiated $\text{CH}_3\text{NH}_3\text{PbI}_3$ perovskite solar cells. *Adv. Electron. Mater.* **2017**, *3*, 1600438. [[CrossRef](#)]
42. Landi, G.; Fahrner, W.R.; Concilio, S.; Sessa, L.; Neitzert, H.C. Electrical hole transport properties of an ambipolar organic compound with Zn-atoms on a crystalline silicon heterostructure. *IEEE J. Electron Devices Soc.* **2014**, *2*, 179–181. [[CrossRef](#)]
43. Laquai, F.; Andrienko, D.; Mauer, R.; Blom, P.W.M. Charge carrier transport and photogeneration in P3HT:PCBM photovoltaic blends. *Macromol. Rapid Commun.* **2015**, *36*, 1001–1025. [[CrossRef](#)] [[PubMed](#)]
44. Landi, G.; Tunc, A.V.; De Sio, A.; Parisi, J.; Neitzert, H.-C. Hole-mobility limits for the $\text{Zn}(\text{OC})_2$ organic semiconductor obtained by SCLC and field-effect measurements. *Phys. Status Solidi A* **2016**, *213*, 1909–1914. [[CrossRef](#)]
45. Pivrikas, A.; Ullah, M.; Sitter, H.; Sariciftci, N.S. Electric field dependent activation energy of electron transport in fullerene diodes and field effect transistors: Gill's law. *Appl. Phys. Lett.* **2011**, *98*, 092114. [[CrossRef](#)]
46. Sze, S.M.; Ng, K.K. *Physics of Semiconductor Devices*, 3rd ed.; Wiley-Interscience: Hoboken, NJ, USA, 2007; ISBN 978-0471143239.
47. Servaites, J.D.; Ratner, M.A.; Marks, T.J. Organic solar cells: A new look at traditional models. *Energy Environ. Sci.* **2011**, *4*, 4410–4422. [[CrossRef](#)]
48. Landi, G.; Barone, C.; Pagano, S.; De Sio, A.; Neitzert, H.C. Investigation of the solvent influence on polymer–fullerene solar cells by low frequency noise spectroscopy. *Can. J. Phys.* **2014**, *92*, 879–882. [[CrossRef](#)]
49. Tsoi, W.C.; Spencer, S.J.; Yang, L.; Ballantyne, A.M.; Nicholson, P.G.; Turnbull, A.; Shard, A.G.; Murphy, C.E.; Bradley, D.D.C.; Nelson, J.; et al. Effect of crystallization on the electronic energy levels and thin film morphology of P3HT:PCBM blends. *Macromolecules* **2011**, *44*, 2944–2952. [[CrossRef](#)]
50. Pivrikas, A.; Juška, G.; Mozer, A.J.; Scharber, M.; Arlauskas, K.; Sariciftci, N.S.; Stubbs, H.; Österbacka, R. Bimolecular recombination coefficient as a sensitive testing parameter for low-mobility solar-cell materials. *Phys. Rev. Lett.* **2005**, *94*, 176806. [[CrossRef](#)] [[PubMed](#)]
51. Deledalle, F.; Shakya Tuladhar, P.; Nelson, J.; Durrant, J.R.; Kirchartz, T. Understanding the apparent charge density dependence of mobility and lifetime in organic bulk heterojunction solar cells. *J. Phys. Chem. C* **2014**, *118*, 8837–8842. [[CrossRef](#)]
52. Li, L.; Tang, H.; Wu, H.; Lu, G.; Yang, X. Effects of fullerene solubility on the crystallization of poly(3-hexylthiophene) and performance of photovoltaic devices. *Org. Electron.* **2009**, *10*, 1334–1344. [[CrossRef](#)]
53. Barone, C.; Pagano, S.; Méchin, L.; Routoure, J.-M.; Orgiani, P.; Maritato, L. Apparent volume dependence of $1/f$ noise in thin film structures: Role of contacts. *Rev. Sci. Instrum.* **2008**, *79*, 053908. [[CrossRef](#)] [[PubMed](#)]



© 2017 by the authors. Licensee MDPI, Basel, Switzerland. This article is an open access article distributed under the terms and conditions of the Creative Commons Attribution (CC BY) license (<http://creativecommons.org/licenses/by/4.0/>).